Wave Propagation in Bubbly Fluids and Cavitation Mitigation

Tianshi Lu
lu@math.wichita.edu

ABSTRACT

We studied the acoustic and shock wave propagation in bubbly fluids using direct numerical simulations (DNS), and estimated the efficiency of the cavitation mitigation using bubbly fluids. Our method is based on the front tracking technique developed for free surface flows. In the simulations, the movement and oscillation of multiple compressible bubbles were tracked simultaneously. Our simulations of the propagation of acoustic and shock waves in bubbly fluids achieved good agreement with theoretical predictions and experiments.

The DNS method for bubbly flows has been applied to the study of cavitation mitigation by bubbly fluids. The pressure wave propagation in the bubbly fluid was simulated, and the collapse pressure of cavitation bubbles was calculated by solving the Keller equation with the liquid pressure obtained from the bubbly flows. The efficiency of the cavitation mitigation by bubble injection has been quantified. The use of layers of nondissolvable gas bubbles as a pressure mitigation technique to reduce the cavitation erosion has been confirmed.

INTRODUCTION

Wave propagation in bubbly fluids has attracted investigators for many decades because of its special properties. Bubbly fluids have the unique feature that even a minute bubble concentration (volume fraction less than one percent) significantly increases the compressibility of the system. The system transports energy at a speed considerably lower than the sound speeds in both phases as a result of the energy exchange between the liquid and the bubbles. When additional effects such as vaporization and condensation play a role, e.g., in cavitating flows, further phenomena, still little understood, are superimposed upon the basic behavior of bubbly flows. The rich internal structure of bubbly flows endows the medium strikingly complex behavior.

One of the reasons for the study of bubbly flows is their wide applications ranging from hydraulic engineering to high energy physics experiments. In particular, we are interested

in a recent application of bubbly fluids in the mitigation of cavitation damages in the Spallation Neutron Source (SNS) (Riemer et al., 2002). Another important motivation is to connect the microscopic behavior of individual bubbles to the macroscopic behavior of the mixed medium that one directly observes. Since the microstructure in this case is made up of a complex substructure, the task is much more complicated than that of classical kinetic theory.

The wave propagation in bubbly fluids has been studied using a variety of mathematical models. Significant progress has been achieved in the study of systems consisting of non-condensable gas bubbles (Wijngaarden, 1972; Caflisch et al., 1985; Beylich and Gülhan, 1990; Watanabe and Prosperetti, 1994) and of vapor bubbles (Finch and Neppirassee, 1973; Hao and Prosperetti, 1999). The treatment of the kinetic and thermal properties of the medium, e.g., the compressibility of the liquid and the thermal conduction, by different authors varies. But they shared a common feature that the two phases were not separated explicitly, i.e., the bubble radius and concentration were considered as functions of time and space. The Rayleigh-Plesset equation or the Keller equation governing the evolution of spherical bubbles has been used as the kinetic connection between the bubbles and fluid. These models include many important physical effects in bubbly systems such as the viscosity, the surface tension and thermal conduction. Numerical simulations of such systems requires relatively simple algorithms and are computational inexpensive.

Nevertheless, homogenized models treat the system as a pseudo-fluid and cannot capture all features of the rich internal structure of the bubbles. They exhibit sometimes large discrepancies with experiments (Watanabe and Prosperetti, 1994) even for systems of non-condensable gas bubbles. Their range of validity is limited to small void fraction and small amplitude waves. These models are also not suitable if the bubbles are distorted severely by the flow or even fission into smaller bubbles, as it may happen in cavitating and boiling flows (Ceccio and Brennen, 1991; Kuhn de Chizelle et al., 1995). The direct numerical simulation (DNS) method, which solves the full nonlinear system of compressible fluid dynamics equations in every component of the multiphase domain, is potentially free of these deficiencies.

DNS is based on techniques developed for free surface flows. Welch (1995) investigated numerically the evolution of a single vapor bubble using interface tracking method. Juric and Tryggvason (1998) simulated the boiling flows using the incompressible flow approximation for both liquid and vapor and a simplified version of interface tracking. Lu et al. (2008) developed an algorithm for the simulation of dynamic phase transitions in compressible fluids, in which the transition was modeled as a tracked jump discontinuity and coupled to acoustic waves. In this paper, we perform DNS simulations of small void fraction bubbly fluids using front tracking for compressible fluid equations. Our FronTier code is capable of tracking and resolving topological changes of a large number of interfaces in two- and three-dimensional spaces. A homogeneous approach to multiphase flows has also been developed in the FronTier code and compared to the DNS approach by Samulyak et al. (2004; 2006). In this paper, both the bubbles and the fluid are compressible because we are interested in the speed of wave propagations. We simulated
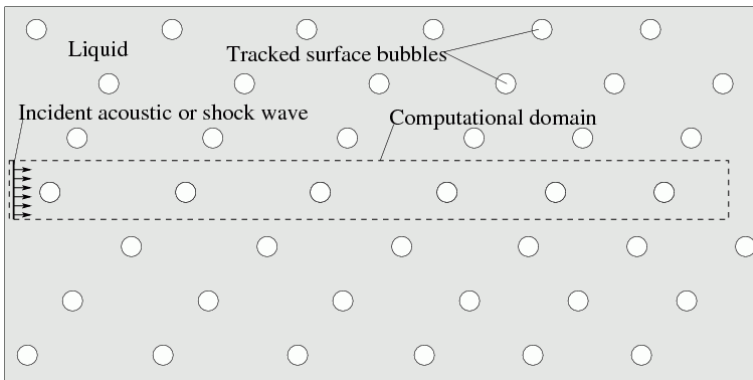
the propagation of acoustic and shock waves in bubbly fluids with small void fraction and compared them with the theory and experiments. After the validation of the FronTier based DNS method for bubbly flows, it was applied to the engineering problem of cavitation mitigation in the Spallation Neutron Source, which involves bubbly flows of relatively large void fraction.

In the following sections, we first go over the governing system of equations and main features of the homogenized model of bubbly flows, then describe the numerical method that we used. After that we present the results of the DNS on linear and shock wave propagation in bubbly fluids along with the comparison to the theory and the experiments. In the subsequent section, after the description of the SNS and the bubble injection technique for the cavitation mitigation, the cavitation is estimated in two steps. First the pressure wave propagation in the mercury target of the SNS is simulated using the front tracking method, and then the collapse pressure of cavitation bubbles is calculated by solving the Keller equation under the ambient pressure whose profile has been obtained in the first step. The efficiency of the cavitation mitigation is estimated by comparing the average collapse pressure with and without injected bubbles. Finally we conclude the paper with a summary of our results.

MATHEMATICAL FORMULATION

In the DNS method, we study bubbly fluids as a system of one-phase domains separated by explicit interfaces, as illustrated in Fig. 1.

Fig. 1. Schematic of numerical experiments on the wave propagation in bubbly fluids.

We solve the system of Euler's equations.

$$\frac{\partial \rho}{\partial t} = -\nabla \cdot (\rho \mathbf{u})$$

$$\rho(\frac{\partial}{\partial t} + \mathbf{u} \cdot \nabla)\mathbf{u} = -\nabla p$$

$$\rho(\frac{\partial}{\partial t} + \mathbf{u} \cdot \nabla)e = -p\nabla \cdot \mathbf{u}$$

$$p = p(\rho, e)$$

The equations are solved separately in each gas bubble and in the ambient liquid subject to the liquid-gas interface conditions. In the equations, **v**, ρ, p and e are the velocity, density, pressure and specific internal energy of the fluid. The continuity of pressure and normal velocity is satisfied at the liquid-gas interface. If the surface tension is important as in surface instability problems, we modify the pressure interface condition by adding a pressure jump due to the surface tension and local curvature. In simulations presented in this paper, the surface tension was neglected as it is important only for bubbles of a sub-micron size. Gas bubbles in simulated fluids are much larger. Notice that we have also neglected the viscosity and heat conduction in fluid equations. These effects are often important in the dynamics of bubbly flows, and will be included in future simulations. We use the polytropic equation of state (EOS) model for gas bubbles, $p = (\gamma\text{-}1)\rho e$, where γ is the ratio of specific heats, and the stiffened polytropic EOS (Lu, 2005) for the ambient liquid.

Wave Equations in Homogenized Models

Since some of our results are compared to the homogenized theory of bubbly fluids, we present in this section main equations. The theory on bubbly flows is based on the homogenized model, in which the fluid and bubbles are treated as a single mixed phase, opposed to the two separated phases in the direct numerical simulations. In compressible fluids with gas bubbles, the conservation of mass and momentum in one spatial dimension give

$$\frac{1}{\rho_f c_f^2}\frac{\partial p}{\partial t} + \frac{\partial u}{\partial x} = \frac{\partial \beta}{\partial t}$$

$$\frac{\partial(\rho u)}{\partial t} + \frac{\partial(\rho u^2 + p)}{\partial x} = 0$$

where β is the bubble volume fraction, ρ is the averaged density of the mixed phase that equals $\beta\rho_g + (1 - \beta)\rho_f$, and p is the averaged pressure. The bubble oscillation in weakly compressible fluids is governed by the Keller equation (Keller and Miksis, 1980), which is an extension of Rayleigh-Plesset equation,

$$\left(1 - \frac{1}{c_f}\frac{dR}{dt}\right)R\frac{d^2R}{dt^2} + \frac{3}{2}\left(1 - \frac{1}{3c_f}\frac{dR}{dt}\right)\left(\frac{dR}{dt}\right)^2 = \frac{1}{\rho_f}\left(1 + \frac{1}{c_f}\frac{dR}{dt} + \frac{R}{c_f}\frac{d}{dt}\right)(p_B - p)$$

The p in the equation coincides with the average pressure in the conservation laws to the lowest order in β (Commander and Prosperetti, 1989). p_B is the liquid pressure at bubble surface. The bubble pressure p_g is approximately uniform except for sound waves of frequency far above the resonance. For air bubbles of diameter 0.1 mm and above, the thermal diffusivity $v = \kappa/(\rho c_p) \ll \omega R^2$ except for sound waves of frequency far below resonance (κ, ρ and c_p are the heat conductivity, density and specific heat with fixed pressure for the gas respectively). Therefore the bubbles are almost adiabatic for near-resonant sound waves. For bubbles consisting of a γ-law gas, $p_g R^{3\gamma}$ is a constant. Neglecting the viscosity, the difference between p_g and p_B is from the surface tension, $p_g = p_B + 2\sigma/R$.

Linear Waves. The following dispersion relation for linear sound waves in bubbly fluids was derived from the wave equations (Wijngaarden, 1972).

$$\frac{k^2}{\omega^2} = \frac{1}{c_f^2} + \frac{1}{c^2}\frac{1}{1 - \frac{i\delta\omega}{\omega_B} - \frac{\omega^2}{\omega_B^2}}$$

where ω_B is the resonant frequency of single bubble oscillation, δ is the damping coefficient accounting for the various dissipation mechanisms. c_f is the sound speed in bubble free fluid, and c is the sound speed in the low-frequency limit, which is given by

$$\frac{1}{c^2} = (\beta\rho_g + (1-\beta)\rho_f)(\frac{\beta}{\rho_g c_g^2} + \frac{1-\beta}{\rho_f c_f^2})$$

where ρ_g and ρ_f are the densities of the gas and the fluid, c_g and c_f are the sound speeds of the two phases. For adiabatic bubbles,
$c^2 = \gamma p/(\beta\rho_f)$, $(\omega_B R)^2 = 3\gamma p/\rho_f$. Chapman and Plesset (1971) formulated δ as the sum of the acoustic, viscous and thermal contributions. It has been pointed out by Prosperetti et al. (1988) and Commander and Prosperetti (1989) that δ depends on the frequency of the sound wave. Nevertheless, Eq. (8) has been widely used for the dispersion relation. The dispersion relation for near-resonant sound waves measured in different experiments (Fox, et al., 1955; Macpherson, 1957; Silberman 1957) agreed with the theoretical predictions.

Shock Waves. The shock profile in the bubbly fluid evolves into a smooth steady form in contrast to the sharp discontinuity in the pure fluid. The steady state shock speed was obtained from the Rankine-Hugoniot relation (Watanabe and Prosperetti, 1994),

$$\frac{1}{U^2} = \frac{1}{c_f^2} + \rho_f\frac{\beta_b - \beta_a}{P_a - P_b}$$

where subscripts a and b stand for ahead and behind the shock front. Since heat conduction and surface tension is neglected, $P_a\beta_a^\gamma = P_b\beta_b^\gamma$. The evolution into a steady wave can take very long time and distance, and the unsteady waves move at higher velocities. The shock profiles were measured for various gas bubbles by Beylich and Gülhan (1990), to which our simulation results will be compared.

NUMERICAL METHOD

In this paper, we study bubbly fluids as a system of one-phase domains separated by free interfaces using FronTier, a front tracking compressible hydrodynamics code. Front tracking is an adaptive computational method in which a lower dimensional moving grid is fit to and follows distinguished waves in a flow. The front propagates according to the dynamics around it (i.e., Lagrangian) while the regular spatial grid is fixed in time (i.e., Eulerian). The discontinuities across the interfaces are kept sharp so as to eliminate the interfacial numerical diffusion which plagues traditional finite difference schemes.

The implementation of the front tracking method in the FronTier code is described in details by Glimm et al. (2002). Here we formulate the main ideas. In each time step, the

front is propagated first, and then the interior states are updated. For the front propagation, each point of the interface is propagated in the normal direction, and the states on either side of the interface are evolved according to the solution of the non-local Riemann problem. The hyperbolic solver has three steps: slope reconstruction, prediction using local Riemann solver, and correction by nonlocal solver. Then the states on the propagated fronts are updated in the tangential direction while the fronts are fixed. After that the fronts are tested for intersection and then untangled or redistributed if necessary to resolve the topological change or the clustering/sparsity of grid points on the interfaces due to front contract/expand.

For the subsequent interior state update, FronTier uses high resolution shock-capturing hyperbolic schemes on a spatial grid. Among the various shock capturing methods currently implemented in FronTier, a second order monotone upwind scheme for conservation laws (MUSCL) scheme developed by Van Leer and adapted for FronTier by I-L. Chern was used for the simulation here. Detailed descriptions of the MUSCL scheme can be found in Collela (1985) and the references therein. The two-pass implementation is used in FronTier, namely, first regular cells then irregular cells update. Different equation-of-state models are used for gas/vapor bubbles and the ambient fluid.

FronTier can handle multidimensional wave interactions in both two- (Glimm et al., 1988) and three- (Glimm et al., 2000) dimensional spaces. Although computationally intensive, front tracking is potentially very accurate in treating many physical effects in bubbly flows, such as the compressibility of the fluid, surface tension and viscosity. Since the FronTier code is capable of tracking simultaneously a large number of interfaces and resolving their topological changes, many effects that are difficult to handle in mathematical models for bubbly flows are now naturally included in the simulations, e.g., the bubbles' deviation from sphericity, bubble-fluid relative motion, bubble merge/fissure, and bubble size/spatial distribution. This approach has numerous potential advantages for modeling the phase transitions in boiling and cavitation flows. We have implemented a model for the phase transitions induced mass transfer across free interfaces (Lu et al., 2008). FronTier is implemented for distributed memory parallel computers.

For the application of FronTier to the simulation of bubbly flows, the region around a long column of bubbles (tens to hundreds) has been chosen as the computational domain, as shown in Fig. 1. Two approximations were used in the simulations. The flow inside the column was assumed to be axisymmetric and the influence from the neighboring bubbles was included by treating the domain boundary as a reflecting wall, which is called the Neumann boundary in FronTier. Thus the wave propagation in bubbly flows was reduced to an axisymmetric two-dimensional problem. An extensive introduction to the FronTier code for axisymmetric flows can be found in Glimm et al. (2002).

We have shown that the assumption of axial symmetry is adequate for the study of main features of the wave propagation in bubbly fluids. This conclusion is based on the comparison of our numerical results with theoretical and experimental data presented in the next section. The axisymmetric assumption is exact for the scattering of the planar

wave by an isolated column of bubbles that are initially spherical. The Neumann boundary condition for the modeling of the presence of other bubbly layers is strong because scattered pressure waves are only partially reflected. As a contrast, the scattering theory, on which the Keller equation is based, completely neglects the reflection between bubbles and the secondary scattering. Therefore the scattering theory only holds for the case of small void fraction such that bubble interaction is negligible. For moderate void fraction, the secondary scattering cannot be neglected, and the Neumann boundary condition between adjacent bubbles is a better approximation.

SIMULATION RESULTS ON BUBBLY FLOWS

In this section, we present the results of the DNS of the linear and shock wave propagations in bubbly fluids. Since the void fraction is small (0.02% for linear waves, 0.25% for shock waves), the homogenized model is expected to be valid. The dispersion relation measured from simulations is compared with theoretical predictions in the subsection on linear waves. Shock speed values measured from simulations are compared to steady-state values, and shock profiles for various gas bubbles are compared to experimental data (Beylich and Gülhan, 1990) in the subsection on shock waves.

Linear Waves

To compare the simulation results with the theory, we measured the dispersion relation. Writing down the complex wave number k in Eq. (8) as $k = k_1 + i k_2$, we have

$$e^{i(kx-\omega t)} = e^{-k_2 x} e^{i(k_1 x - \omega t)}$$

from which the phase velocity of the sound wave is defined as $V = \omega/k_1$, and the attenuation coefficient α in dB per unit length is defined as $\alpha = 20 \log_{10} e \cdot k_2$. The bubble radius in the simulation was $R = 0.06$ mm. The resonant frequency is

$$f_B = \frac{1}{2\pi R} \sqrt{\frac{3\gamma p}{\rho_f}} = 54.4 \text{ KHz}$$

We simulated the sound waves of frequencies ranging from 30 to 300 KHz. The volume fraction was $\beta = 0.02\%$. The amplitude of the pressure wave was chosen to be 0.1 bar, one tenth of the ambient pressure. The linearity was ensured by performing numerical simulations with sound waves of half amplitude which gave virtually the same dispersion relation.

For each frequency, the sound wave of up to 8 wavelengths was propagated from the pure fluid into the bubbly region. The cross sectional averaged pressure in the bubbly region was recorded at selected times and positions, from which the phase velocity and the attenuation coefficient were measured. The phase velocity was obtained by measuring the propagation speed of the first pressure node in the bubbly region. The envelope of the oscillating pressure wave was plotted and the attenuation coefficient was measured in the 1cm-long bubbly fluid region next to the incident plane by fitting the envelope to an
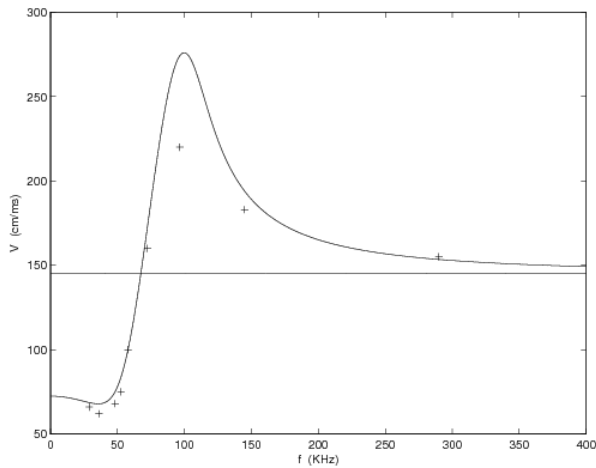
exponential curve. A shorter region was used for the frequency with the strongest attenuation (λ = 2cm).

Table 1. Phase velocities (V) and attenuation coefficients (α) from simulation and theory. λ is the wavelength in pure water. V and α are the simulation results, V_{th} and α_{th} are the theoretical predictions from Eq. (8) with $\delta = 0.7$, $R = 0.06$ mm, $\beta = 0.02\%$.
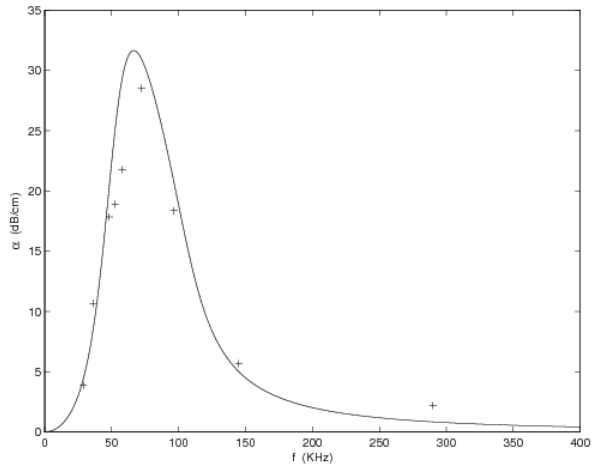
λ (cm)	f (KHz)	V (cm/ms)	V_{th} (cm/ms)	α (dB/cm)	α_{th} (dB/cm)
0.5	290	155	153	2.2	0.9
1.0	145	183	194	5.7	5.0
1.5	96.7	220	274	18.4	20.7
2.0	72.5	160	173	28.5	30.9
2.5	58.0	100	100	21.8	29.4
2.75	52.7	75	84	18.9	25.2
3.0	48.3	68	75	17.8	20.4
4.0	36.3	62	68	10.7	8.5
5.0	29.0	66	69	3.9	4.4

The phase velocities and attenuation coefficients measured from the simulations are listed in Table 1 along with theoretically predicted values. Theoretical values were calculated using the damping coefficient $\delta = 0.7$ in Eq. (8). There are various theoretical and empirical formulas for the damping coefficient (Wijngaarden, 1972), several of them giving value under 0.1. The parameters in our simulations is closest to those in experiment of Fox et al. (1955), who used the empirical value of 0.5 for the damping coefficient. The measured dispersion relation was compared to the theoretical curve in Fig. 2(a). It can be seen that the simulation agrees well with the theory. However, the point in Fig. 2(a) with frequency about 100 KHz has large deviation from the theoretical value. Most likely the deviation is due to the dependence of δ on the frequency, especially near the resonance as pointed out in by Prosperetti et al. (1988).

Fig. 2. Comparison of the dispersion relation between the simulation and the theory. $R = 0.06$ mm, $\beta = 0.02\%$. The crosses are the simulation data and the solid line is the theoretical prediction from Eq. (8) with $\delta = 0.7$. The horizontal line in figure (a) is the sound speed in pure water.
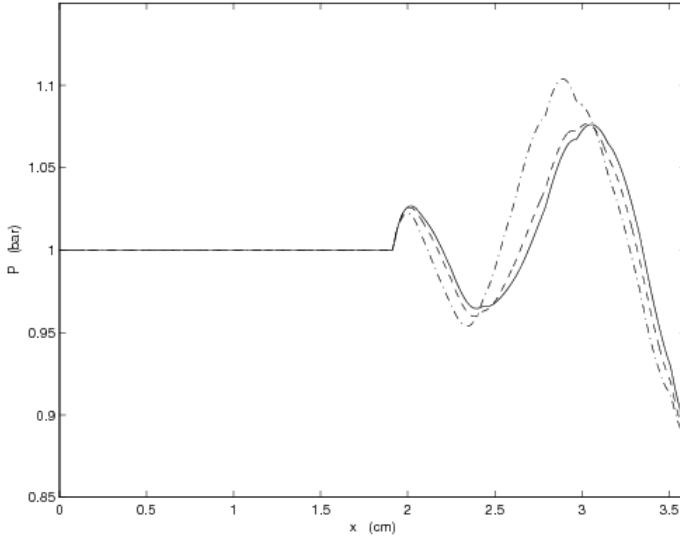
(a)　Phase velocity　　　　　　　　　　　(b) Attenuation coefficient

The grid resolution for most of our simulations on linear wave propagations was 100 grids per millimeter. To ensure the accuracy of the simulation results, a mesh refinement check has been carried out. Fig. 3 shows a typical result. It can be seen that the results were reasonably accurate at the default grid resolution (100 grids/mm). The one dimensional grid on the bubble surface, which is the explicitly tracked fluid interface, was more refined, the circumference of a bubble in the simulation was discretized into 50 points. The approximation of cylindrical domain has been justified by varying the aspect ratio of the cylinder containing a bubble, which confirms that the dispersion relation only depends on the void fraction, i.e., the ratio of the bubble volume over the cylinder volume, but not on the aspect ratio.

Fig. 3. The pressure profile in bubbly water 23 microseconds after the incidence of the sound wave with wavelength 1 cm in pure water. The default resolution used in the simulations was 100 grids/mm, under which the bubble radius $R = 0.06$ mm corresponds to 6 grids. Solid line is the default resolution 100 grids/mm, dash-dotted line is 50 grids/mm, and dashed line is 200 grids/mm.
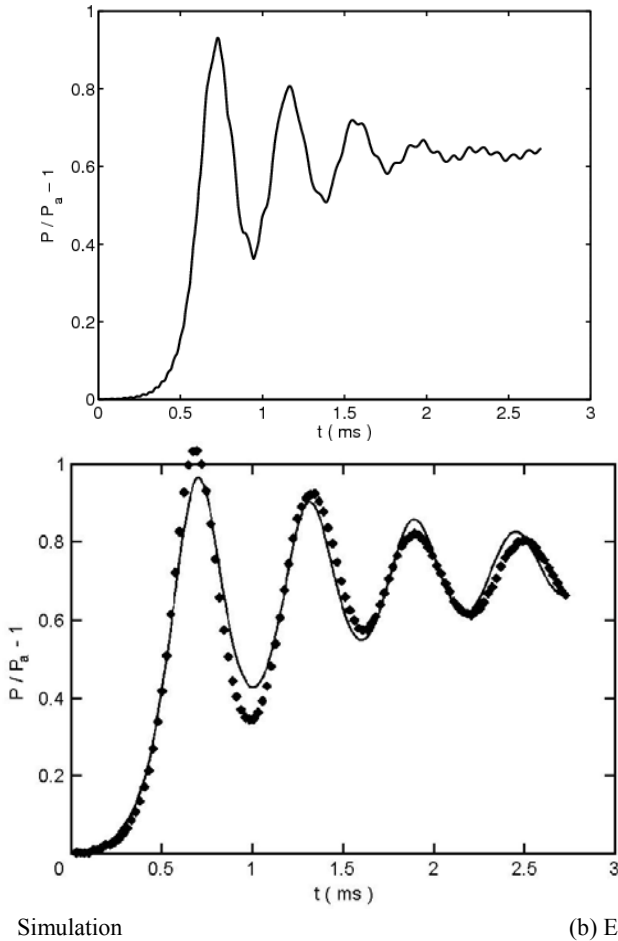

Shock Waves

Beylich and Gülhan (1990) studied the propagation of shock waves in glycerol filled with bubbles of various gases. We carried out numerical simulations using their experimental settings. We have also varied the sound speed in the pure fluid to measure the corresponding shock speeds and compared them to the steady-state values given by Eq. (10). In the simulations, the pressure behind the shock was either fixed at the boundary or set as the initial pressure in an air layer next to the bubbly fluid. The results from the two methods have been compared and found to be very close.

The measured shock speeds are listed in Table 2. The speeds were measured about 10 cm away from the shock incident plane. It is seen from the table that the measured shock speeds differ from the steady state values by less than 15%. The reason for the deviation is that the shock waves in simulations had not reached the steady state.

Table 2. Shock speeds measured from the simulations are compared to the steady state values. β_a is the bubble volume fraction ahead of the shock, P_b is the pressure behind the shock, U is the measured shock speed, and U_{th} is the corresponding steady-state value given by Eq. (10). $P_a = 1.11$ bar, $\rho_f = 1.22$ g/cm^3, $R_a = 1.15$ mm.

gas(γ)	c_f (m/s)	β_a (%)	P_b (bar)	U (m/s)	U_{th} (m/s)
SF$_6$ (1.09)	1450	0.25	1.9	26.20	25.40
SF$_6$ (1.09)	458	0.25	1.9	22.52	22.48
SF$_6$ (1.09)	145	0.25	1.9	13.47	12.64
N$_2$ (1.4)	1450	0.25	1.7	25.56	26.68
N$_2$ (1.4)	458	0.25	1.7	22.21	23.35
N$_2$ (1.4)	145	0.25	1.7	12.29	12.79
He (1.67)	1450	0.25	1.9	25.68	30.01
He (1.67)	458	0.25	1.9	22.69	25.49
He (1.67)	145	0.25	1.9	13.52	13.11
SF$_6$ (1.09)	1450	2.17	1.8	8.72	8.52
SF$_6$ (1.09)	458	2.17	1.8	8.04	8.39
SF$_6$ (1.09)	145	2.17	1.8	7.10	7.35
N$_2$ (1.4)	1312	2.17	1.8	8.60	9.42
N$_2$ (1.4)	458	2.17	1.8	9.09	9.25
N$_2$ (1.4)	145	2.17	1.8	7.80	7.92
He (1.67)	1450	1.04	1.9	13.92	14.96
He (1.67)	458	1.04	1.9	12.70	14.29
He (1.67)	145	1.04	1.9	9.70	10.44

Fig. 4. The shock profiles in glycerol filled with SF_6 bubbles. The parameters in the simulations were from the experiments. $P_a = 1.11$ bar, $P_b = 1.80$ bar, $\rho_f = 1.22$ g/cm^3, $R_a = 1.15$ mm, $\gamma = 1.09$ and $\beta = 0.25\%$. The curve in the experimental figure is the original fitting with artificial turbulent viscosity by Beylich and Gülhan (1990).

(a) Simulation   (b) Experiment

The shock profiles were measured at 1.0 m away from the shock incident plane as in the experiments of Beylich and Gülhan (1990). The shock profiles for SF_6 bubbles of volume fraction 0.25% are plotted in Fig. 4. These figures show that the pressure in the bubbly fluid oscillated after the passage of the shock front. The oscillation amplitude from the simulation was close to the experimental value. However the oscillation period from the simulation was 28% shorter than the experimental value.

There were several sources of error that could be responsible for the deviation. The main source of error was numerical dissipation at the bubble surface. The default grid resolution for the simulations on shock wave propagation was 100 grids per centimeter,

and the bubble circumference contains about 100 points. It has been found that increasing resolution only slightly changed the oscillation amplitude and period. Other sources of error include the axisymmetric approximation and the Neumann boundary condition on the domain wall. It is worth mentioning that the oscillation period calculated by Watanabe and Prosperetti (1994) based on the homogenized model was also about 1/4 shorter than the experimental value.

The shock profiles with various gas bubbles and different volume fractions were measured and they agreed with the experiments as well. The oscillation amplitude was found to be smaller for gas with larger polytropic index γ, and the oscillation period was longer for larger bubble volume fraction β, both of which agreed with the experiments. As a summary, the shock velocity measurement agreed well with the theory, while the shock profiles agreed with the experiment qualitatively and partly quantitatively.

According to Noordzij and van Wijngaarden (1974), waveforms observed during the propagation of shocks in bubbly liquids can be classified into three types, referred to as A-, B-, and C-type waves. The highly oscillatory A-type waveform is usually found near the boundary at which the shock is introduced. The other two represent later stages in the evolution of the wave. As pointed out by Watanabe and Prosperetti (1994), the heat exchange between bubbles and liquid plays an important role in the formation of B- and C-type shocks. Due to the negligence of heat diffusion in our simulations, we only observed A-type shocks. Our simulations agreed with Beylich and Gülhan's experiments (1990), in which they only published data on A-type shocks. We have already implemented a heat diffusion algorithm in FronTier (Lu, 2005), and will explore all types of shock profiles in the future.

APPLICATION TO CAVITATION MITIGATION

The comparison of simulation results with theory and experiments in the previous section validated the FronTier based DNS method for bubbly flows. The DNS method is used in this section to study the cavitation reduction problem in the Spallation Neutron Source target container. The DNS method is well suited for the description of bubbly flows in the SNS target since large void fraction fluids and very strong pressure waves make the applicability of the homogenized theory questionable.
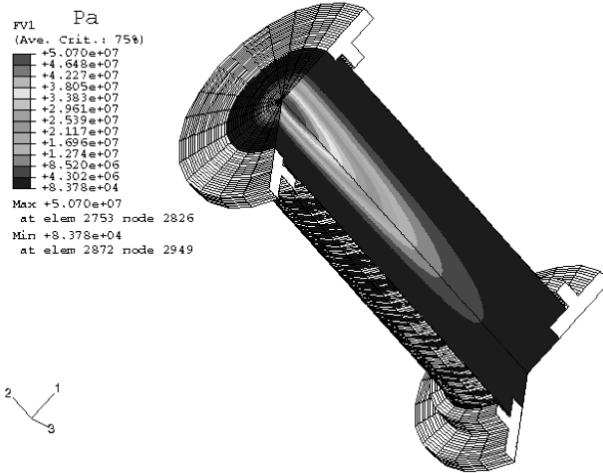
First we introduce the design of the SNS target and the associated fluid dynamical issue, followed by a description of our method of approach. Then we analyze the simulation results on the pressure wave propagation in the pure and bubbly mercury, and calculate the collapse pressure of cavitation bubbles. We conclude by an estimation of the cavitation mitigation efficiency via bubbly injection.

Spallation Neutron Source

The Spallation Neutron Source (SNS) is an accelerator-based neutron source being built at Oak Ridge National Lab. The SNS will provide the most intense pulsed neutron beam in the world for scientific research and industrial development. In SNS, 800 MeV proton beams bombarding the mercury target in a steel container deposit totally 2.1 kJ of energy per pulse in less than 300 ns which results in the rapid pressure increase in the mercury (see Fig. 5). The peak deposited energy density is 19 J/cc, corresponding to 500 bar in mercury. The subsequent pressure waves induce severe cavitation on the container, so much so that the lifetime of the container was only two weeks with 1MW proton pulses at the frequency of 60 Hz (Riemer et al., 2002). In order to mitigate the cavitation erosion, research is being done on the evaluation of cavitation-resistant materials and coatings. It has also been suggested that the injection of non-dissolvable gas bubbles into the container could absorb the energy of the pressure wave. Our goal is to estimate the efficiency of the cavitation mitigation by the bubble injection method.

The SNS target prototype tested at the Los Alamos National Laboratory is a cylinder of 10 cm diameter and 30 cm length. The pressure in the target is about 1 bar in the absence of the proton beam. After the proton beam bombards the target, the pressure rises in the mercury almost instantaneously compared to acoustic time scales. The pressure distribution, as shown in Fig. 5, has a Gaussian profile in the transverse direction with $\sigma = 1.0$ cm and an exponential attenuation along the axis. The pressure profile is $P_0(r, z) = 500\exp(-r^2 - 0.1z)$, where r and z are in cm, and the origin of the z-axis is the window where proton beams enter. When non-dissolvable gas bubbles are injected into the container, the bubble pressure has little change after the proton pulse and it remains about 1 bar.

Fig. 5. The pressure distribution right after a pulse of proton beams in the mercury target of the Spallation Neutron Source. Courtesy of SNS experimental facilities, Oak Ridge National Lab.

Method of Approach

Before we compare the cavitation erosion in pure and bubbly mercury, a brief introduction to the mechanism of cavitation damage and the method we used to quantify it is given in this section. Cavitation is the process in which bubbles, consisting of vapor and non-condensable gas, form, expand, and collapse in the fluid according to the surrounding pressure which decreases and increases rapidly. Vapor bubbles are formed when the pressure falls below the saturated vapor pressure of the fluid at the ambient temperature or some critical pressure smaller than the corresponding saturation pressure (Brennen, 1995). They implode when the fluid pressure rises back above the saturated vapor pressure or when the bubbles move into a region with higher pressure. If the bubble is close to the container wall, the shock wave from the rebound of the collapse erodes the wall as in the SNS target container.

The attenuation of the pressure wave during the rebound phase of the cavitation bubbles was studied extensively in by Hickling and Plesset (1964). The pressure of the rebounded wave that hits the container wall can be used to quantify the cavitation erosion. Since it is proportional to the first collapse pressure of cavitation bubbles, we only need to compare the average collapse pressure in the pure mercury and the bubbly mercury for the estimation of the cavitation mitigation efficiency. In order to calculate the collapse pressure, we need to know how the cavitation bubbles grow and collapse under the pressure wave in the container. Since the collapsed bubble size (< 0.1 μm) is less than a millionth of the container size (10 cm), it is difficult to simulate directly the evolution of cavitation bubbles in the entire container. Instead we estimated it in two steps.
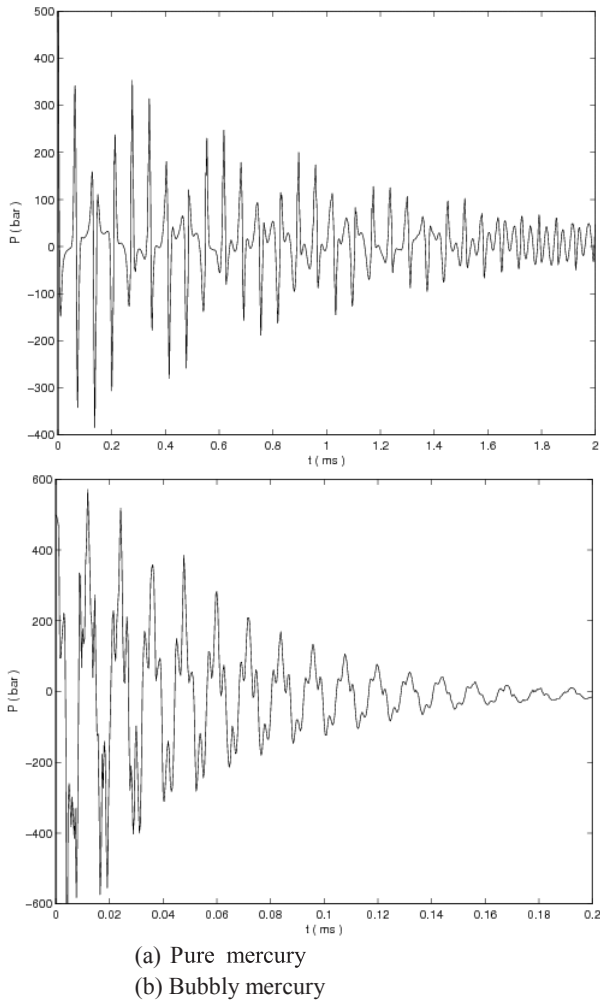
First, we simulated the propagation of pressure waves in the container caused by the initial pressure profile. The simulation was carried out for both the pure mercury and mercury containing non-dissolvable gas bubbles. For the simulation of the bubbly mercury, the bubble surfaces were tracked explicitly via the front tracking method described in the previous sections. The pressure relaxation caused by the cavitation was ignored in the simulation of pressure waves in the container. We assumed that the growth and collapse of cavitation bubbles is uncorrelated, namely that the far field liquid pressure for a cavitation bubble is not significantly perturbed by relaxation waves from neighboring cavitation bubbles. Since the distribution of cavitation centers is unknown for mercury under such conditions, accounting for pressure relaxation processes would contain a large amount of uncertainty.

In the second step, the collapse pressure of cavitation bubbles was calculated by solving the Keller equation under the liquid pressure whose profile was obtained in the first step. A cavitation bubble consists of vapor and non-condensable gas. Due to the liquid - vapor phase transition, the partial vapor pressure in a bubble remains negligible compared to the amplitude of pressure waves in the SNS target, while the partial pressure of the gas (typically air) changes violently. As a result, it suffices to calculate the growth and collapse of cavitation bubbles that consist only of air for the estimation of the collapse pressure.

Pressure Wave Propagation in the Container

Inferred from for the initial pressure profile, the strongest pressure oscillation and consequently the most severe cavitation might be located at the center of the entrance window, which was confirmed by the simulation. Therefore we compared the pressure profile at the window center in the pure and bubbly mercury. The pressure profile in the pure mercury is shown in Fig. 6(a), while the pressure profile in the mercury filled with air bubbles is shown in Fig. 6(b).

Fig. 6. The computed pressure profiles at the center of the entrance window. The pressure profile in pure mercury is compared against that in the mercury injected with non-condensable gas bubbles of radius 1.0 mm and volume fraction 2.5%.

(a) Pure mercury
(b) Bubbly mercury

It is readily seen that, as expected, the pressure decayed much faster in the bubbly mercury, since bubbles absorbed the energy from pressure waves and spread it away from the entrance window. The pressure oscillation in the bubbly mercury was also more rapid due to reflections between the window and bubbles. The typical decay time in both cases is shorter than the period between two proton pulses at the frequency of 60 Hz. Both profiles can be approximately described by the following formula

$$P_{w(t)} = P_{w0} e^{-\frac{t}{\tau}} \cos\left(\frac{2\pi t}{T}\right)$$

where P_{w0} is the pressure oscillation amplitude on the window right after the bombard of the proton pulse, τ is the inverse of the attenuation rate, and T is the oscillation period. Numerical values of the coefficients are $P_{w0} = 500$ bar, $\tau = 0.94$ ms, $T = 70$ μs for pure mercury and $P_{w0} = 600$ bar, $\tau = 50$ μs, $T = 12$ μs for mercury filled with air bubbles of radius 1.0 mm and volume fraction 2.5%.

We compared the result of direct numerical simulation with that of the multiple scattering theory. The homogenized wave equations (5) and (6) were solved numerically in the longitudinal direction of the chamber with the given initial liquid pressure profile. As recognized by Caflisch et al. (1985), Eqs. (5) and (6) are valid for small void fractions and accurate up to the first order of β. In our simulation for the SNS problem, $\beta = 2.5\%$, which is not very small. Therefore, the simulation results could be different from the theoretical predictions based on homogenized wave equations. Indeed we found discrepancies, for example, for injected air bubbles of radius 1.0 mm and volume fraction 2.5%, the simulation showed an oscillation with period $T = 12$ μs, while the homogenized wave equations gave a period of 15.4 μs. The simulated frequency is higher due to the nonlinear effect of a finite void fraction. In another example, where $\beta = 0.53\%$ and $R = 0.5$ mm, the simulation had an oscillation period $T = 16$ μs, while the theory gave a period of 17.6 μs, which is still different but closer to the simulation result because the void fraction is smaller in this case. Another reason for the discrepancy is the high frequency of the pressure wave in the liquid.

Eqs. (5) and (6) were derived for sound waves with $\lambda \gg R$. In the SNS problem, the energy deposition from the proton beam increases the liquid pressure to about 500 bar at the entrance window, while the pressure in the injected bubbles remains around 1 bar. At finite bubble volume fraction, the induced pressure wave has a wavelength of the same order as the bubble radius. These effects make DNS a valuable method in the study of the SNS problem and a more general class of bubbly flows.

The accuracy of the results has been guaranteed by mesh refinement check. Thanks to the relatively large void fraction, we were able to use higher resolution in simulations of bubble layers in SNS than in those of linear and shock waves. Due to the exponential decay of proton beams along their path, the energy deposition has longitudinal attenuation. In the presence of the attenuated deposition, standing wave does not form in the container, which is confirmed by numerical simulations. Furthermore, simulations showed that the longitudinal attenuation was strengthened by injected bubbles due to energy absorption, such that a 3-cm layer of bubbles near the entrance window is effectively the same as a chamber full of bubbles in terms of pressure damping.

Collapse Pressure of Cavitation Bubbles

The second step is the calculation of the collapse pressure of cavitation bubbles. The Keller equation for the bubble growth and collapse in the weakly compressible liquid was used for that purpose. With the ambient liquid pressure obtained in the first step, the closed system of equations is Eq. (7) with $p_g = p_B + 2\sigma/R$ and $p_g R^3 = p_{g0} R_0^3$. The
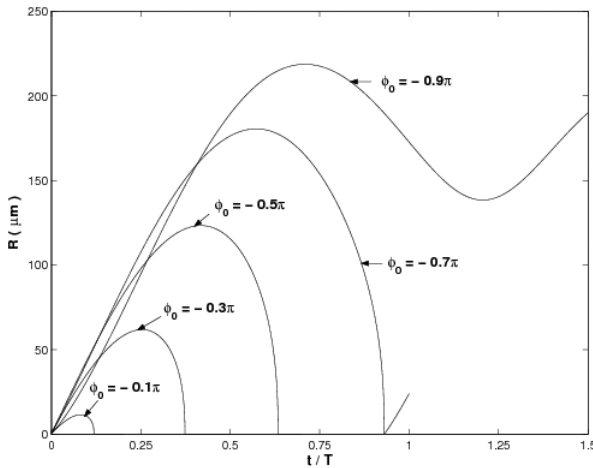
pressure p is the difference between the ambient pressure and the vapor pressure of mercury in the bubble. However the latter is much smaller in our case and can be neglected. The gas pressure in the bubble is associated with the bubble radius by the isothermal relation, which is valid for most of the cavitation bubbles in the target, especially during their evolution stages after the formation and before the collapse. To estimate the range of initial bubble sizes for our numerical studies, recall that the cavitation bubble grows from a nucleus whose radius is bounded below by the stability condition (Arndt, 1981), $4\sigma/(3R_0) < -p$. For liquid mercury, $\sigma = 0.48$ kg/s^2, in SNS a typical tension of 100 bar gives $R_0 > 0.065$ μm. Therefore it is reasonable to assume that the initial radius of most cavitation bubbles in SNS is below 1 μm, which justifies the isothermal relation for the bubbles.

The pressure waves in both the pure and bubbly mercury have an attenuating sinusoidal form. Since the attenuation is much slower than the period of oscillation, we calculated the overall collapse pressure of cavitation bubbles by using a purely sinusoidal pressure wave for one period and summing up all periods with the attenuating amplitude. The purely sinusoidal time-wise fluctuation of pressure has the following form,

$$p(t) = P \sin \left(\frac{2\pi t}{T} + \phi_0 \right)$$

where ϕ_0 is the initial phase when a cavitation bubble starts to grow from a nucleus. ϕ_0 must be between $-\pi$ and 0 because for the bubbles to grow the initial pressure must be below the saturated pressure of mercury, which is almost 0 compared to the pressure wave in the SNS target.
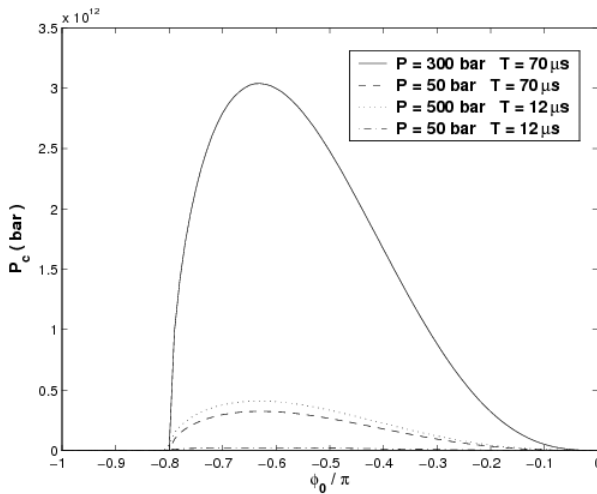
Fig. 7. Bubble size evolution with different ϕ_0. $R_0 = 1.0$ μm, $p_{g0} = 0.01$ bar, $P = 100$ bar, $T = 20$ μs.

The typical bubble size evolutions with various ϕ_0 are shown in Fig. 7. It's interesting to notice that the bubble does not always collapse -- the bubbles beginning to grow at $\phi_0 < -0.8\pi$ continues to grow after a period. Although they may collapse after two or

more periods according to the Keller equation, the associated collapse pressure is smaller since the ambient pressure has attenuated. On the other hand, for ϕ_0 between -0.8π and 0 a bubble collapses within about a period. We are only interested in the first collapse because it produces the largest pressure peak and after that the bubble often fissures into a cloud of tiny bubbles and the Keller equation no longer applies (Brennen, 1995). Fig. 8 shows the dependence of the first collapse pressure P_c on ϕ_0. It is seen that the collapse pressure is highest for ϕ_0 around -0.63π, and the average collapse pressure $\overline{P_c}$ is roughly one half of the peak value at $\phi_0 = -0.63\pi$.

Fig. 8. The first collapse pressure P_c vs. ϕ_0 under the sinusoidal pressure waves with different amplitude P and period T. The solid line and the dashed line correspond to the pure mercury; the dotted line and the dash-dotted line correspond to the mercury filled with air bubbles of radii 1.0 mm and volume fraction 2.5%.

Neglecting the surface tension and the viscosity, which is justified by the high pressure wave in the liquid, the Keller equation becomes a purely acoustic equation so that P_c is a function of $R_0/c_f T$. In prescribed ambient pressure wave, P_c is a function of R_0 and p_{g0}, and we observed that P_c depends only on the gas content $p_{g0}R_0^3$ as long as $p_{g0} \ll P$. Combining the two observations, we see that $\overline{P_c}$ is a function of P and $p_{g0}(R_0/c_f T)^3$. In fact, in the range of $P < 10$ Kbar and $T < 1$ ms, an empirical formula for $\overline{P_c}$ with P, T as variables and p_{g0}, R_0 as parameters was obtained,

$$\overline{P_c}(P,T) = 46.5 \left(\frac{P}{\rho_f c_f^2}\right)^{1.25} \left(\frac{p_{g0}}{\rho_f c_f^2}\left(\frac{R_0}{c_f T}\right)^3\right)^{-0.50} \text{Kbar}$$

with error less than 1%. The result agreed with the fact that the higher rate of stressing the fluid is experiencing, the higher tension can be sustained. In the bubble injection regime, the period of pressure oscillation T decreases which in turn reduces the cavitation bubble collapse pressure.

Efficiency of Cavitation Damage Mitigation

Our goal is to evaluate the mitigation of the cavitation damage by the bubble injection, i.e., to find the ratio between the overall impact on the container from the collapses of cavitation bubbles in the pure mercury and the mercury with non-dissolvable gas bubbles. We needed only to compare the average collapse pressure $\overline{P_c}$. According to Eq. (15), $\overline{P_c}$ can be factored into two parts, one depending on P and T, and the other on p_{g0} and R_0. This implies that the ratio between the two cases (with and without bubble injection) is independent of the size of the initial nucleus and amount of gas in it as long as $p_{g0} \ll P$.

To estimate quantitatively the efficiency of the cavitation mitigation on the entrance window by the bubble injection, we found the average collapse pressure in each period and took the sum over all the periods of the attenuating sinusoidal pressure wave given in Eq. (14). In other words, we defined

$$S = \sum_{n=0}^{\infty} \overline{P_c}(P_w(nT), T) = \sum_{n=0}^{\infty} \overline{P_c}(P_{w0} e^{-\frac{nT}{\tau}}, T)$$

where the summand is the average collapse pressure in the n'th period. The overall cavitation damage is proportional to S. The mitigation efficiency is defined to be the ratio of S in pure mercury to that in bubbly mercury, i.e., $E(\beta, R) = S(\beta = 0)/S(\beta, R)$, where β and R are the volume fraction and mean radius of the injected bubbles. Combining Eqs. (15) and (16), we obtain

$$S = K P_{w0}^{1.25} T^{1.50}/(1 - e^{-1.25T/\tau})$$

where K is a coefficient depending only on the cavitation nucleus and cancels in $E(\beta, R)$.

Using the data in the paragraph following Eq. (13), we found that $E(\beta = 2.5\%, R = 1.0 \text{ mm}) = 32.7$. Varying β and R in the simulation of pressure wave propagation we can easily measure the corresponding efficiency. For example, when $\beta = 0.53\%$ and $R = 0.5$ mm, we found $P_{w0} = 450$ bar, $\tau = 44$ μs, $T = 16$ μs, and $E(0.53\%, 0.5 \text{ mm}) = 42.9$.

Therefore, we have confirmed the mitigation of cavitation through the injection of non-dissolvable gas bubbles. The bubbles absorb/disperse the energy and rapidly attenuate the pressure on the entrance window of the SNS target so that the cavitation lasts for much shorter time. The simulation results will be compared to experimental data from the SNS group on bubble injection and cavitation mitigation once they are available.

CONCLUSION

Through the comparison of numerical simulations with experiments and theoretical predictions on the propagation of acoustic and shock waves in bubbly fluids, the direct approach to the simulation of bubbly flows using the method of front tracking and the FronTier code has been validated. The method has a variety of current and prospective applications, such as Rayleigh-Taylor instability (Glimm et al., 2001; Jin et al., 2005) and boiling or cavitating flows (Lu et al., 2008). In Xu et al. (2006), the dynamics of vapor

bubble phase boundaries was resolved in the simulations of atomization of a high speed jet, and the tracking of the bubble surfaces was extended to dynamically created bubbles.

The pressure wave relaxation in bubbly mercury in the SNS target has been investigated numerically using the FronTier hydro code. The estimation of cavitation bubble collapse pressure under periodic ambient pressure has been carried out systematically. The efficiency of the mitigation of overall cavitation damage by the injection of bubbles has been calculated. The overall cavitation damage has been found to be reduced by more than an order of magnitude through the injection of gas bubbles with volume fraction of order 1%. Therefore the use of layers of non-dissolvable gas bubbles as a pressure mitigation technique to reduce the cavitation erosion has been confirmed.

REFERENCES

Arndt (1981), "Cavitation in Fluid Machinery and Hydraulic Structures", *Ann. Rev. Fluid Mech.,* Vol. 13, pp. 273-328.

Beylich and Gülhan (1990), "On the Structure of Nonlinear Waves in Liquids with Gas Bubbles", *Phys. Fluids A*, Vol. 2(8), pp. 1412-1428.

Brennen (1995), *Cavitation and Bubble Dynamics*, Oxford University Press.

Caflisch, Miksis, Papanicolaou and Ting (1985), "Effective Equations for Wave Propagation in Bubbly Liquids", *J. Fluid Mech.*, Vol. 153, pp. 259-273.

Ceccio and Brennen (1991), "Observations of the Dynamics and Acoustics of Traveling Bubble Cavitation", J. Fluid Mech., Vol. 233, pp. 633-660.

Chapman and Plesset (1971), "Thermal Effects in the Free Oscillation of Gas Bubbles", ASME J. Basic Eng., Vol. 93, pp. 373-376.

Collela (1985), "A Direct Eulerian MUSCL Scheme for Gas Dynamics", SIAM J. Sci. Stat. Comput., Vol. 6(1), pp. 104-117.

Commander and Prosperetti (1989), "Linear Pressure Waves in Bubbly Liquids: Comparison between Theory and Experiments", J. Acoust. Soc. Am., Vol. 85(2), pp. 732-746.

Finch and Neppiras (1973), "Vapor Bubble Dynamics", J. Acoust. Soc. Am., Vol. 53, pp. 1402-1410.

Fox, Curley and Larson (1955), "Phase Velocity and Absorption Measurements in Water Containing Air Bubbles", J. Acoust. Soc. Am., Vol. 27(3), pp. 534-539.

Glimm, Grove, Li and Tan (2000), "Robust Computational Algorithms for Dynamic Interface Tracking in Three Dimensions", SIAM J. Sci. Comput., Vol. 21, pp. 2240-2256.

Glimm, Grove and Zhang (2002), "Interface Tracking for Axisymmetric Flows", SIAM J. Sci. Comput., Vol. 24(1), pp. 208-236.

Glimm, Grove, Lindquist, McBryan and Tryggvason (1988), "The Bifurcation of Tracked Scalar Waves", SIAM J. Sci. Statist. Comput., Vol. 9, pp. 61-79.

Glimm, Grove, Li, Oh and Sharp (2001), "A Critical Analysis of Rayleigh-Taylor Growth Rates", J. Comput. Phys., Vol. 169, pp. 652-677.

Hao and Prosperetti (1999), "The Dynamics of Vapor Bubbles in Acoustic Pressure Fields", Phys. Fluids, Vol. 11(8), pp. 2008-2019.

Hickling and Plesset (1964), "Collapse and Rebound of a Spherical Bubble in Water", Phys. Fluids, Vol. 7(1), pp. 7-14.

Jin, Liu, Lu, Cheng, Glimm and Sharp (2005), "Rayleigh-Taylor Mixing Rates for Compressible Flow", Phys. Fluids, Vol. 17, pp. 024104-024113.

Juric and Tryggvason (1998), "Computation of Boiling Flows", Int. J. Multiphase Flow, Vol. 24, pp. 387-410.

Keller and Miksis (1980), "Bubble Oscillations of Large Amplitude", J. Acoust. Soc. Am., Vol. 68, pp. 628-633.

Kuhn de Chizelle, Ceccio and Brennen (1995), "Observations and Scaling of Traveling Bubble Cavitation", J. Fluid Mech., Vol. 293, pp. 99-126.

Lu (2005), "Direct Numerical Simulation of Bubbly Flows and Interfacial Dynamics of Phase Transitions", Ph. D. Thesis, Stony Brook University.

Lu, Xu, Glimm, Samulyak and Ji (2008), "Dynamic Phase Boundaries for Compressible Fluids", SIAM J. Sci. Comput., Vol. 30, pp. 895-915.

Macpherson (1957), "The Effects of Gas Bubbles on Sound Propagation in Water", Proc. Phys. Soc. London, Vol. B70, pp. 85-92.

Noordzij and Wijngaarden (1974), "Relaxation Effects, Caused by Relative Motion, on Shock Waves in Gas-bubble/Liquid Mixture", J. Fluid Mech., Vol. 66, pp. 115-143.

Prosperetti, Crum and Commander (1988), "Nonlinear Bubble Dynamics", J. Acoust. Soc. Am., Vol. 83, pp. 502-514.

Riemer et al. (2002), "Status Report on Mercury Target Related Issues", Technical Report No. SNS-101060100-TR0006-R00, Oak Ridge National Laboratory, TN.

Samulyak, Lu and Prykarpatskyy (2004), "Direct and Homogeneous Numerical Approaches to Multiphase Flows and Applications", Lecture Notes in Computer Science, Vol. 3039, pp. 653-660.

Samulyak, Prykarpatskyy, Lu, Glimm, Xu and Kim (2006), "Comparison of Heterogeneous and Homogenized Numerical Models of Cavitation", Int. J. Multiscale Comp. Eng., Vol. 4, pp. 377-390.

Silberman (1957), "Sound Velocity and Attenuation in Bubbly Mixtures Measured in Standing Wave Tubes", J. Acoust. Soc. Am., Vol. 29(8), pp. 925-933.

Watanabe and Prosperetti (1994), "Shock Waves in Dilute Bubbly Liquids", J. Fluid Mech., Vol. 274, pp. 349-381.

Welch (1995), "Local Simulation of Two-phase Flows Including Interface Tracking with Mass Transfer", J. Comp. Phys., Vol. 121, pp. 142-154.

Wijngaarden (1972), "One-dimensional Flow of Liquids Containing Small Gas Bubbles", Ann. Rev. Fluid Mech., Vol. 4, pp. 369-396.

Xu, Kim, Lu, Oh, Glimm, Samulyak, Li and Tzanos (2006), "Discrete Bubble Modeling of Unsteady Cavitating Flow", Int. J. Multiscale Comp. Eng., Vol. 4, pp. 601-616.